

A COMPARISON OF UIT FAR-ULTRAVIOLET AND H α STAR FORMATION RATES

ERIC F. BELL AND ROBERT C. KENNICUTT, JR.

Steward Observatory, University of Arizona, 933 N. Cherry Ave., Tucson, AZ 85721, USA

ACCEPTED BY APJ: 16th October 2000

ABSTRACT

We have used archival ultraviolet (UV) imaging of 50 nearby star-forming galaxies obtained with the Ultraviolet Imaging Telescope (UIT) to derive integrated near-UV and far-UV magnitudes, and have combined these data with H α , far-infrared, and thermal radio continuum measurements to explore the consistency of UV and H α star formation rates (SFRs). In agreement with previous studies, we find that the UV and H α SFRs are qualitatively consistent, even before corrections for extinction are applied. The uncorrected UV SFRs are systematically lower by a factor of 1.5 (with a factor of two scatter) among luminous galaxies with SFR $\gtrsim 1 M_{\odot} \text{ yr}^{-1}$, indicating a higher effective attenuation of the far-UV radiation. Among less luminous galaxies there is no significant offset between the H α and far-UV SFR scales. This behavior is consistent with those of higher-redshift samples observed by Sullivan et al., Glazebrook et al., and Yan et al. for comparable ranges of galaxy luminosities and absolute SFRs. Far-infrared and thermal radio continuum data available for a subset of our sample allow us to estimate the attenuation in the UV and at H α independently. The UV and H α attenuations appear to be correlated, and confirm systematically higher attenuations in the UV. Although the galaxies in our sample show modest levels of attenuation (with median values of 0.9 mag at H α and 1.4 mag at 1550 Å), the range across the sample is large, ~ 4 mag for H α and $\gtrsim 5$ mag in the far-UV (1550 Å). This indicates that the application of a single characteristic extinction correction to H α or UV SFRs is only realistic for large, well-defined and well-studied galaxy samples, and that extinction bias may be important for UV or emission-line selected samples of star-forming galaxies.

Subject headings: galaxies : general — galaxies : photometry — galaxies : stellar content — galaxies : evolution — ultraviolet : galaxies — dust, extinction

1. INTRODUCTION

Until recently most of our information about the systematic behavior of star formation rates (SFRs) in normal nearby galaxies has been based on measurements of the H α emission line (e.g. Kennicutt & Kent 1983; Gallego et al. 1995). In contrast, SFRs for $z > 1$ galaxies are primarily based on observations of the redshifted ultraviolet (UV) continuum (e.g. Madau, Pozzetti, & Dickinson 1998; Steidel et al. 1999). Comparable UV observations for nearby galaxies are being accumulated (e.g. Donas et al. 1987; Tresse & Maddox 1998; Buat et al. 1999; Sullivan et al. 2000), and these have made it possible to derive the cosmic evolution of the volume-averaged SFR in a self-consistent manner. However, questions remain about the systematic accuracy of the UV-derived SFRs, both in terms of the absolute SFR scale and possible redshift-dependent biases in that scale. Similar questions also apply to the H α -based SFRs, and with the extension of this technique to high-redshift galaxies by several groups (e.g. Glazebrook et al. 1999; Yan et al. 1999; Moorcroft et al. 2000) it is important to understand the limitations of this technique also.

Although H α and UV measurements are now available for samples of hundreds of galaxies in each case, there have been only a few direct comparisons of the respective SFRs for galaxies in common. Comparisons of three samples of high-redshift galaxies ($z = 0.7 - 2.2$) by Glazebrook et al. (1999), Yan et al. (1999), and Moorcroft et al. (2000) show that the uncorrected H α fluxes yield SFRs that are ~ 3 times higher than derived from the 2800 Å UV flux. The simplest explanation for this difference would be a systematically higher extinction in the UV. However, similar comparisons using nearby samples present a less clear picture. Buat, Donas, & Deharveng (1987) and Buat (1992) compared balloon-based UV and ground-based H α measurements of small samples of galaxies and found a general

consistency between the extinction-corrected SFR scales. Furthermore, Buat & Xu (1996) estimated UV extinctions for a large sample of star-forming spirals and estimated typical extinctions that are comparable to or lower than those at H α . The most comprehensive comparison to date of UV and H α -based SFRs was carried out by Sullivan et al. (2000), who analyzed balloon-based UV (2000 Å) and H α fluxes for 273 galaxies in the redshift range $0 < z < 0.5$. The galaxies in this sample span nearly 4 orders of magnitude in SFR, ranging from dwarfs to massive spirals; many galaxies are undergoing intense star formation bursts. Although they observed a strong correlation between UV and H α -derived SFRs, they also found that the UV/H α flux ratio decreases significantly with increasing SFR. In low-SFR systems the UV fluxes consistently yield *higher* SFRs than H α , while the reverse is true for galaxies with the highest SFRs. They attribute most of the differences to rapid variability in the SFR over the lifetimes of the starbursts.

These results underscore the need for a complimentary comparison of UV and H α SFRs for a sample of well-resolved nearby galaxies with a fuller range of star formation histories. In this paper we primarily compare far-UV (FUV) and H α SFRs for a sample of 50 nearby star-forming galaxies imaged using the Ultraviolet Imaging Telescope (UIT; Stecher et al. 1997). This sample is much smaller than that studied by Sullivan et al. (2000) but it has several advantages which complement the strengths of their study. The UIT sample is far from complete: rather, it was selected to span a full range of morphological types, luminosities, SFRs, and star formation properties, with the bulk of the sample composed of high-luminosity spiral galaxies. This virtually eliminates the problem of rapidly variable SFRs that are important when analyzing starburst galaxy samples, and allows us to compare the zeropoints of the UV and H α -based SFR scales on a self-consistent basis. Another

advantage of this sample is the availability of truly integrated UV and $H\alpha$ fluxes, which eliminates any possible effects of aperture undersampling at $H\alpha$.

This paper concentrates on a comparison of the integrated fluxes and SFRs of the UIT/ $H\alpha$ sample. Our main objectives are to: 1) compare the SFRs derived from FUV and $H\alpha$ luminosities, with and without corrections for dust attenuation; 2) compare the behavior of our UV/ $H\alpha$ SFRs with those derived for other samples at low and high redshift; and 3) obtain insight into the amount of attenuation suffered by FUV and $H\alpha$ in this sample of star-forming galaxies. Future papers will compare the UV and emission-line properties of individual star-forming regions in these galaxies.

In this paper we follow the convention of Gordon et al. (2000) in using the term ‘attenuation’ to refer to the net loss of radiation from a galaxy at a given wavelength. For a point source such as a star this would be the equivalent to the extinction (itself a combination of dust absorption and scattering), but for a galaxy the radiation reaching the observer is the result of a complicated radiative transfer across multiple lines of sight with enormous variations in local optical depth. In the specific context of this paper it will generally refer to the correction factor that must be applied to the observed integrated UV or $H\alpha$ flux to derive the actual SFR due to the effects of interstellar dust (and exclusive of other physical effects such as escape of ionizing photons from a galaxy, etc.).

The remainder of the paper is organized as follows. In §2, we present the data: near-UV (NUV) and FUV magnitudes, $H\alpha$ line luminosities, far-infrared (FIR) luminosities and thermal radio continuum fluxes at 1.4 GHz. We also present the SFR calibrations for $H\alpha$ and FUV luminosities. In §3, we compare the raw $H\alpha$ and FUV SFRs, and interpret the discrepancies in terms of variations in star formation histories and differences in dust attenuation. In §4, we examine the role of attenuation in more detail. Finally, in §5, we present our conclusions.

2. DATA

Our analysis is primarily based on a sample of 50 nearby star-forming galaxies imaged in the FUV by the UIT. The UIT provides well-resolved (FWHM $\sim 3''$), wide-field (field radius $\sim 40'$) images in both the NUV and FUV. This spatial resolution is useful, as it allows us to evaluate the effects of local processes in determining the global FUV fluxes (e.g. Marcum et al. 2000; Kuchinski et al. 2000).

2.1. FUV Data

The FUV data was taken from the UIT archive at the Multimission Archive at the Space Telescope Science Institute. As part of the Astro payload, the 38-cm UIT flew on two Space Shuttle missions in 1990 Dec and 1995 Mar. For the purposes of this analysis, we selected star-forming spiral and irregular galaxies with sizes comparable to or smaller than the UIT field size (therefore excluding the Large and Small Magellanic Clouds, M31, and M33 from our sample). We also excluded from our analysis E/S0 galaxies with no evidence of massive star formation (the UV emission in such objects is thought to arise from evolved stellar populations), and we excluded galaxies for which the bulk of the $H\alpha$ emission arises from a Seyfert or LINER nucleus (e.g. NGC 2992, NGC 3227, NGC 4151). Two other galaxies, NGC 1268 and UGC 2665 were omitted from the sample because they were not detected in the FUV and no $H\alpha$, far-infrared (FIR) or radio fluxes are available in

any case. Most of the sample galaxies are luminous later-type spirals: the remaining galaxies are split between earlier type spirals, irregulars and starbursting galaxies. The starbursts in this sample are relatively faint compared to those of e.g. Calzetti et al. (1994).

The properties of the galaxies in our sample are summarized in Table 1. Listed are the galaxy name, coordinates, type, distance, distance reference, and Galactic foreground extinction in the V band, as estimated by Schlegel, Finkbeiner, & Davis (1998). When a direct distance determination was not available it was derived using $H_0 = 75 \text{ km s}^{-1} \text{ Mpc}^{-1}$. Note that most of the conclusions of this paper are distance independent as they rely only on flux ratios: only the absolute magnitude and SFR axes in Fig. 2 are affected by distance uncertainties.

Every galaxy was imaged in at least one of the two wide FUV passbands used by the UIT: passband B1 ($\lambda_{\text{eff}} \sim 1521 \text{ \AA}$; $\Delta\lambda \sim 354 \text{ \AA}$) and passband B5 ($\lambda_{\text{eff}} \sim 1615 \text{ \AA}$; $\Delta\lambda \sim 225 \text{ \AA}$). The latter filter was used during daylight observations to exclude dayglow emission lines (Waller et al. 1995). Additional observations in the NUV from the Astro-1 mission were also analyzed when available. These were made in passband A1 ($\lambda_{\text{eff}} \sim 2488 \text{ \AA}$; $\Delta\lambda \sim 1147 \text{ \AA}$). Table 2 lists the filters and exposure times for the specific observations that were analyzed in this paper. We usually chose the longest exposure images with the best signal-to-noise, with exposure times ranging between ~ 250 s and ~ 1500 s.

The UIT imaged galaxies using an image intensifier, recording the images on photographic film. The images have been linearized, flat-fielded, flux-calibrated and distortion-corrected (the e versions of the images). Where possible, we used images which were also astrometrically aligned (the g versions of the images); however, either version of the images produces identical results. Before performing photometry, we manually removed any foreground or background objects, or instrumental artifacts such as scratches or cosmic ray hits. A small subset of the images also contained low-level ‘stripes’, and these were removed by fitting a Gaussian function to the profile of the ‘stripe’ (cf. Kuchinski et al. 2000). Any residuals from this fitting process were found to be comparable to or weaker than variations in the background photographic fog level, and thus they did not contribute significantly to the overall error budget. We refer the reader to Stecher et al. (1997) for more details on the UIT data products.

Integrated fluxes for the galaxies were measured from the calibrated images, using the IRAF¹ task PHOT. Magnitudes were calculated assuming:

$$m_{\text{UV}} = -21.1 + 2.5 \log_{10}(f) \quad (1)$$

where f is the flux in $\text{ergs s}^{-1} \text{ cm}^{-2} \text{ \AA}^{-1}$ (Stecher et al. 1997). The sky level was estimated using an annulus around the galaxy, or in the case of galaxies which were large enough to fill a significant portion of the frame, using boxes in areas which were free of galaxy emission. Our raw FUV and NUV magnitudes are presented in Table 3, along with the aperture used to determine the magnitudes.

The errors in these magnitudes are dominated by uncertainties in measuring the background level of the images. These uncertainties were estimated by performing photometry on blank areas of the program image using the same sized apertures as for the galaxy, or in the case of large galaxies, by using the

¹IRAF is distributed by the National Optical Astronomy Observatories, which are operated by the Association of Universities for Research in Astronomy, Inc., under cooperative agreement with the National Science Foundation.

dispersion in the average sky levels measured in 20×20 pixel (22.4×22.4 arcsec) boxes, in order to measure the background variation on different spatial scales. The scaling factors between these dispersions and the error in the aperture photometry were derived empirically from cases where both were available. These were found to be larger than expected from Poisson statistics by approximately a factor of four, indicating that the errors are correlated on large spatial scales (not unexpected given the nonlinear nature of the photographic detector used with UIT). This algorithm reproduces the errors in the blank-sky aperture photometry to better than a factor of two, over a large range of aperture area. Other sources of error, including pixel-to-pixel noise, imperfect masking foreground and background objects, or cosmetic feature residuals are much smaller than the error in the background fitting discussed above.

We devoted a considerable effort to testing for errors due to nonlinearity in the calibrated data. Our tests show that any residual nonlinearity at high surface brightness is unimportant for the images used in our analysis. However, comparisons of long and short-exposure images of the same fields show a significant nonlinearity at faint levels, with discrepancies of $\sim 20\%$ at exposure levels lower than 50 ADU (Stecher et al. 1997). Our own tests confirmed this effect, but we also found a significant variation in the magnitude of the nonlinearity within the data set; therefore we cannot derive an appropriate correction for this effect. The net effect of the nonlinearity is to underestimate the total flux in short-exposure images by up to 0.2 mag when compared to long-exposure images. We avoided this problem by not using the short-exposure images in our analysis. However the same effect, if present, would also cause us to underestimate the UV fluxes in the long-exposure images, if a significant fraction of the emission arises from low surface brightness regions. Our tests demonstrate that all but the brightest galaxies have significant contributions from these regions, and this may lead to a systematic underestimate of the UV fluxes by between 0.1 and 0.2 mag.

We have compared our photometry with published FUV data. We constructed a weighted average of the B1 and B5 magnitudes (where available), and adopted this as a representative FUV magnitude. As a check of our internal accuracy, we have compared our magnitudes with those derived from the same images by Waller et al. (1997). The mean zeropoints of the two sets of magnitudes are identical, with a median difference from galaxy to galaxy of 0.14 mag. The RMS difference is substantially larger (0.44 mag), but when two highly discrepant galaxies are excluded the RMS deviation is 0.24 mag. We believe that the differences largely reflect the careful background fitting in our analysis, though the typical estimated uncertainties in our UV magnitudes are still larger than ± 0.1 mag.

In Figure 1 we compare our magnitudes with independently measured FUV magnitudes from other instruments: OAO-2 (1650 Å; Code & Welch 1982), FAUST (1550 Å; Deharveng et al. 1994), SCAP (2000 Å; Donas et al. 1987) and FOCA (2000 Å; Donas et al. 1990). We have also compared our magnitudes with ‘total’ extrapolated FUV magnitudes from Rifatto et al. (1995). In summary, we find reasonable agreement with the raw magnitudes from the literature, but with a mean offset of -0.23 ± 0.07 mag (excluding NGC 3034, which is very faint in the FUV and has a steep UV spectrum, due to strong extinction effects, so the comparison for NGC 3034 is highly passband dependent). We believe that the offset, which is significant at the 3σ level, is due primarily to aperture effects in the

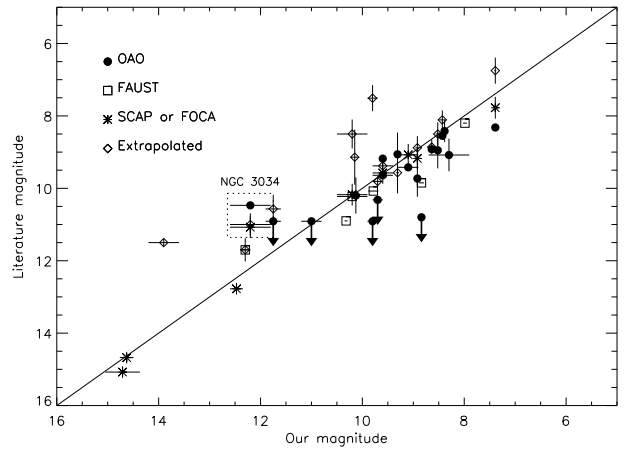


FIG. 1.— Comparison of our total FUV UIT magnitudes with total FUV magnitudes from the literature, assuming a common zero point of -21.1 . We compare with the magnitudes from 4 UV telescopes: OAO (solid circles), FAUST (open squares), SCAP and FOCA (asterisks). We also compare with the extrapolated ‘total’ FUV magnitudes of Rifatto et al. (1995, open diamonds). NGC 3034 (M82) is indicated separately: because it is so highly reddened, its FUV flux is highly passband-dependent.

published magnitudes, many of which were derived from apertures smaller than or comparable to the galaxy sizes (Rifatto et al. 1995). This interpretation is supported by our comparison with the ‘total’ extrapolated magnitudes of Rifatto et al. (1995). We find good agreement between most of their magnitudes and ours, with a standard deviation of ~ 0.2 mag and no offset. We do find, however, that some of the largest galaxies in our sample have FUV magnitudes which strongly differ (by up to 2.5 mag) from Rifatto et al. (1995). However almost all of those cases involved very large extrapolations of IUE fluxes (measured in $10'' \times 20''$ apertures) to ‘total’ magnitudes in the Rifatto et al. database. This underscores the need to exercise extreme care when applying UV data from the literature. In summary, we find that our magnitudes are accurate to ~ 0.2 – 0.4 magnitudes, with no significant offset from the literature calibrations, once aperture effects have been taken into account.

The FUV magnitudes in Table 3 are used later to calculate SFRs. The latter are calibrated in terms of luminosity per unit frequency, so we converted the FUV absolute magnitudes (which are based on F_λ) to F_ν , assuming an effective wavelength for the B1 and B5 filters of $\lambda_{\text{eff,FUV}} = 1567$ Å (this is accurate to better than $\pm 6\%$). We corrected this flux for Galactic extinction following Schlegel et al. (1998), and adopting the Galactic extinction curve of Gordon, Calzetti & Witt (1997).

Later, to increase the galaxy sample size, we include 33 galaxies observed by the balloon-based FAUST telescope (Deharveng et al. 1994) at 1650 Å with existing literature H α fluxes. These data have somewhat larger FUV uncertainties, and are subject to modest aperture effects. These data are not a primary focus of this paper (so they are not included in the tables of galaxies), but are simply included to confirm the trends observed with the UIT galaxies with an independent sample of galaxies.

2.2. H α , Radio Continuum, and Far-Infrared Data

The primary goal of this paper is to compare FUV and H α SFRs, and explore the effects of dust on both of these indicators. Consequently, we compiled measurements of the inte-

grated fluxes of the galaxies in $H\alpha$, radio continuum, and FIR (as a probe of dust content). The data, as discussed below, are listed in Table 4. The table also lists total absolute V magnitudes and the sources of the $H\alpha$, radio, and FIR data. The V magnitudes and the $H\alpha$ fluxes have been corrected for Galactic extinction following Schlegel et al. (1998).

The $H\alpha$ fluxes come from a wide variety of sources in the literature. In many cases more than one source was available, and in these cases a weighted average was derived, with double weight given to fluxes derived from CCD imaging (as opposed to photoelectric aperture photometry). A few of the fluxes were measured from unpublished CCD imaging obtained by the authors, and are published here for the first time. These images have been flux-calibrated and were continuum-subtracted using scaled narrow-band continuum images. Some of the data were obtained with narrowband filters which included only the $H\alpha$ line, but most were obtained with broader filters which also included the $[N II] \lambda 6548, 6583$ lines. In many cases the average $[N II]/H\alpha$ flux ratio has been measured from published $H II$ region spectrophotometry, or from integrated spectra of the galaxies (Kennicutt 1992). Otherwise, for 40% of the galaxies, the $H\alpha + [N II]$ fluxes have been corrected for contamination by the $[N II] \lambda 6583$ line following the prescription of Kennicutt (1983). Total fluxes were multiplied by a factor of 0.75 for spirals and 0.93 for types Sm and later. Note that use of this correction is a conservative assumption: adoption of a constant $[N II]$ fraction would serve to enhance the trend in $H\alpha$ to FUV ratio which we explore later in §3.

In §4 we also use the thermal radio continuum from a subset of our sample of galaxies to investigate the behavior of the attenuation at $H\alpha$. The integrated radio continuum flux of a galaxy is a typically a combination of non-thermal radio emission from cosmic-ray electrons and supernova remnants (with typically a steep spectral index $S_\nu \propto \nu^{-0.8}$, roughly) and thermal bremsstrahlung emission from electrons in ionized gas (with a much shallower spectral index $S_\nu \propto \nu^{-0.1}$). Unfortunately the non-thermal component is dominant at centimeter wavelengths, typically accounting for more than 90% of the total flux at 1.4 GHz (Condon 1992; Niklas et al. 1997). Consequently the thermal fraction can only be measured by obtaining matched-beam multi-frequency observations, fitting the non-thermal spectrum at low frequencies and extracting the (small) thermal component. Reliable data are only available for a small sample of galaxies, and for fewer yet among our sample. For our analysis we have derived thermal radio fluxes at 1.4 GHz, using thermal fractions at 1 GHz derived by Niklas et al. (1997) in conjunction with the radio luminosities from the literature. Niklas et al. (1997) carefully decomposed the thermal and nonthermal components of the radio spectra of 74 galaxies with radio fluxes at a minimum of 4 frequencies using a two component fit. This sample includes 13 galaxies in common with our sample, with thermal fractions significant at better than 1σ . We have added a thermal fraction at 1.465 GHz for DDO 50 from Tongue & Westpfahl (1995), a thermal fraction at 4.9 GHz for NGC 925 from Duric, Bourneuf, & Gregory (1988), and a thermal flux at 92 GHz for M82 taken from Carlstrom & Kronberg (1991) and discussed at length in Condon (1992). Total radio continuum fluxes for our sample with thermal fractions were available between 1.4 and 1.5 GHz: we translated these fluxes to a 1.4 GHz flux using a typical spectrum for a non-thermal continuum dominated source ($S_\nu \propto \nu^{-0.8}$).

FIR fluxes from the Infrared Astronomical Satellite (IRAS)

have been compiled and translated into total 8–1000 μm fluxes using the method of Gordon et al. (2000). The 12 μm , 25 μm , 60 μm and 100 μm fluxes were numerically integrated to provide an estimate of the 8–120 μm flux. The 60 μm and 100 μm fluxes were then used to define a dust temperature for a $\beta = 1$ dust emissivity model to extrapolate to 1000 μm . The total IR flux determined in this way is typically 1.9 ± 0.4 times larger than the FIR estimator of Helou et al. (1985) which was designed to measure the bulk of the FIR flux from a galaxy (the range in the ratio of total IR to FIR estimator is 0.8–3.3).

The FUV, $H\alpha$, thermal radio, and FIR fluxes were translated into total luminosities and powers using the distances listed in Table 1. These luminosities, along with the absolute V band magnitude, are presented in Table 4. The typical uncertainties in the $H\alpha$ and FIR luminosities are $\pm 20\%$. The uncertainties in the thermal radio powers are more variable and usually larger: the radio errors listed in Table 4 are derived directly from the quoted errors in the thermal fractions.

2.3. SFR Calibrations

Before comparing the SFRs derived from FUV and $H\alpha$, we must first translate the galaxy luminosities into SFRs using the appropriate conversions. In this paper we adopt the calibrations of Kennicutt (1998) for the FUV and $H\alpha$ SFRs:

$$SFR(M_\odot \text{ yr}^{-1}) = 1.4 \times 10^{-28} L_{\text{FUV}} (\text{ergs s}^{-1} \text{ Hz}^{-1}), \quad (2)$$

$$SFR(M_\odot \text{ yr}^{-1}) = 7.9 \times 10^{-42} L_{H\alpha} (\text{ergs s}^{-1}), \quad (3)$$

For the purposes of this analysis the absolute SFR scales are less important than adopting a consistent set of calibrations for the two different methods. Both calibrations assume a Salpeter (1955) initial mass function (IMF) between 0.1 M_\odot and 100 M_\odot . The overall absolute SFR scale does depend on IMF (at a factor of a few level at most for plausible IMFs), but the important point is that the relative comparison of $H\alpha$ and FUV SFRs is quite robust. The $H\alpha$ and FUV luminosities at a given age depend primarily on the shape of the upper IMF over a modest range in mass and are independent of the shape of the lower mass end of the IMF. For realistic ranges of upper IMF slopes the $H\alpha$ to FUV ratio should not vary by more than $\sim 30\%$ (e.g. Glazebrook et al. 1999).

The $H\alpha$ line provides a virtually instantaneous measure of the SFR, since the dominant ionizing population consists of OB stars with lifetimes of < 10 Myr. However the stars contributing to the luminosity of a galaxy at 1550 \AA cover a much wider range of ages, so the SFR calibration must explicitly assume a SFR history over the past 100 Myr or longer. The calibration in eq. (2) assumes continuous star formation over timescales in excess of 100 Myr, an approximation which is most appropriate for a large galaxy with essentially constant star formation when averaged over the entire disk. However this conversion is reasonably robust to variations in the recent star formation history, as long as it has been reasonably continuous when averaged over periods of tens of Myr. For more discussion of the calibrations and their uncertainties, see Kennicutt (1998).

3. COMPARISON OF UNCORRECTED STAR FORMATION RATES

We first compare the FUV and $H\alpha$ SFRs, uncorrected for extinction, in Figure 2. The left panel compares the FUV and $H\alpha$ SFRs directly for 39 of the 50 UIT galaxies (solid circles) and for 33 galaxies observed using FAUST (Deharveng et al. 1994) with $H\alpha$ data from the literature (open circles). In addition, data for a sample of 107 FUV selected galaxies with $0 < z < 0.5$

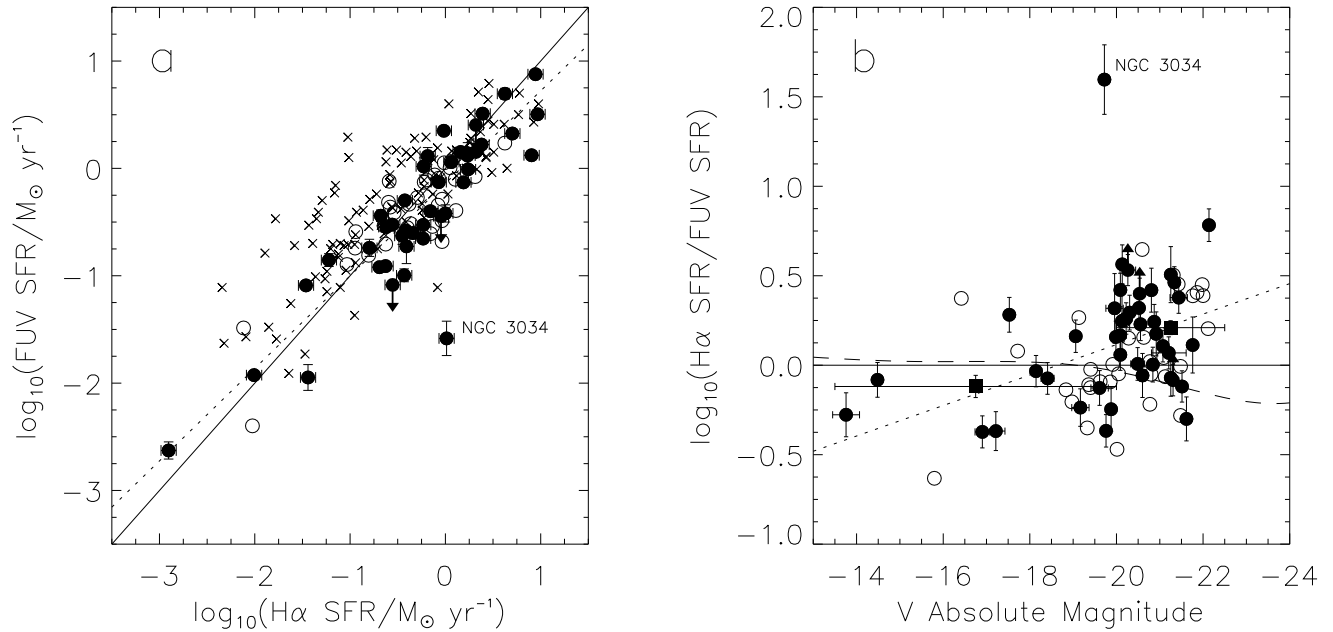


FIG. 2.— Comparison of uncorrected FUV and $H\alpha$ SFRs. The left panel shows a direct comparison of FUV and $H\alpha$ SFRs for UIT galaxies (solid circles), FAUST galaxies (open circles) and FUV selected galaxies from Sullivan et al. (crosses). The right panel shows the $H\alpha$ to FUV SFR ratio as a function of absolute magnitude. Arrows denote FUV upper limits, and the solid lines denote equal SFRs, if the calibrations in equations (2–3) are used. Filled squares denote the mean ratios for galaxies in two luminosity ranges, as described in the text. The dotted line shows the best fit to the variation of $H\alpha$ to FUV SFR ratio with absolute magnitude (dotted line). The dashed line denotes the expected trend in $H\alpha$ to FUV SFR ratio (arbitrarily normalized to zero at $M_V = -20$) expected from metallicity effects alone (Zaritsky et al. 1994; Sullivan et al. 2000).

from Sullivan et al. (2000) is shown by crosses. These galaxies are not included explicitly in the following quantitative discussion, and are plotted only to allow later comparison between our study and Sullivan et al. (2000). The right panel displays the $H\alpha$ to FUV SFR ratio as a function of V -band absolute magnitude for the UIT and FAUST data (solid and open circles respectively). A few UIT galaxies have only upper-limit FUV fluxes, and they are denoted by arrows in the figure. The solid line in both panels corresponds to equal UV and $H\alpha$ SFRs, using the calibrations in equations (2) and (3) respectively. The first clear result is that uncorrected $H\alpha$ and FUV SFRs are qualitatively consistent with each other over three and a half orders of magnitude in SFR and nearly two orders of magnitude in V band luminosity. With the exception of NGC 3034 (M82), the $H\alpha$ and FUV SFRs for the UIT and FAUST data are generally consistent, with an average offset of 0.08 ± 0.04 dex, in the sense that the $H\alpha$ SFRs are $\sim 20\%$ higher than the UV-derived SFRs on average. The RMS dispersion is 0.28 dex (a factor of 1.9), significantly higher than would be expected from the uncertainties in the individual SFRs.

Figure 2 also shows a significant trend in the ratio of $H\alpha$ to FUV SFRs with absolute magnitude. Although our sample is small, a Spearman rank correlation test shows that the departure is significant at greater than the 99.9% level. If we divide the sample at $M_V = -20$, the $H\alpha$ to FUV ratio for the lower luminosity galaxies is -0.10 ± 0.05 dex as compared to $+0.18 \pm 0.04$ dex for the more luminous subsample. This corresponds to a difference (between the lower and higher luminosity galaxies) of a factor of two.

This systematic change in the $H\alpha$ /FUV SFR ratio with SFR and galaxy luminosity is qualitatively consistent with the previ-

ous findings of Sullivan et al. (2000) and our results provide additional insights into the origin of this effect. The FUV and $H\alpha$ data analyzed by Sullivan et al. (2000) were obtained with mismatched apertures, and the authors expressed some concern that aperture sampling effects might account for part of the trend in $H\alpha$ /FUV ratio. However, our data are largely free of aperture bias and we observe a qualitatively similar trend in $H\alpha$ /FUV SFR ratio (panel a of Fig. 2), which argues for a physical origin for the trend.

However, our results do differ from those of Sullivan et al. (2000) in a few respects. The uncorrected FUV SFRs of low SFR galaxies from Sullivan et al. (2000) are larger than the raw $H\alpha$ SFRs by factors of a few: this led Sullivan et al. (2000) to the conclusion that the effects of bursts in SFR dominate their data. The $H\alpha$ emission traces the SFR over the past 5–10 Myr, whereas the UV flux reflects a weighted average of the SFR over the past ~ 100 Myr. If the evolution of a dwarf galaxy is characterized by brief bursts (duration $\ll 100$ Myr) separated by relatively long quiescent periods, then one will tend to observe most of the galaxies between bursts, when the $H\alpha$ luminosity will yield a systematically lower SFR relative to the UV emission. This effect is not seen at a significant level in our sample. It is likely that the differing behaviors of the samples is due to the different selection criteria. Sullivan et al. (2000) selected galaxies in the FUV (favoring galaxies with increased present day SFRs). On the other hand, the UIT imaged a sample of well-known, often optically-bright galaxies (optical selection would less weight on recent star formation). Because the UIT selection is relatively ill-defined, we do not attempt to quantitatively address the different selection biases between the UIT sample and that of Sullivan et al. (2000); however, it is clear

that FUV selection would favor the inclusion of a large population of preferentially UV-bright starbursting galaxies. Another possibility is that modest evolution takes place between $0 < z < 0.5$ in the lowest SFR galaxies only (e.g. Broadhurst, Ellis, & Shanks 1988; Lilly 1993). Metallicity effects on the $H\alpha$ and FUV emission of the stars are unlikely to account for any of the trend. More luminous galaxies tend to possess systematically higher metal abundances (Zaritsky et al. 1994); but, as Sullivan et al. (2000) discuss, the models of Leitherer et al. (1999) show that higher abundances tend to *reduce* the ionizing luminosity relative to the FUV brightness (dashed line in Fig. 2), contrary to the trend observed in Fig. 2.

In low-luminosity galaxies the uncorrected UV-based SFRs are systematically higher than those measured from $H\alpha$ by $25\% \pm 12\%$. If this were to be explained by differential extinction effects it would require a *lower* attenuation of the UV radiation relative to $H\alpha$, a counter-intuitive result made all the more unlikely by the generally low extinctions observed in most dwarf galaxies. As mentioned earlier, Sullivan et al. (2000) suggested that the higher UV/ $H\alpha$ ratios are due to temporal variations in the SFR in these low-luminosity galaxies. This scenario fits in well with observations of dwarf galaxy star formation histories, which suggest large variations in SFR over the galaxy's lifetime (e.g. Dohm-Palmer et al. 1998; Tolstoy et al. 1998). Although our sample is far too small to test the scenario directly, it provides a plausible explanation for our observations also. However, note that it is difficult to rule out inconsistencies in the SFR calibration at this level (e.g. §2.3 Kennicutt 1998).

In higher luminosity galaxies the trend is reversed, i.e. the uncorrected $H\alpha$ luminosities yield SFRs that are on average 50% larger than those derived from the uncorrected FUV fluxes. Sullivan et al. (2000) also observed this trend, attributing it to temporal effects; in this case postulating that the most luminous $H\alpha$ -emitting galaxies are preferentially observed at the peak of the starburst, when the $H\alpha$ luminosity is expected to yield a systematically higher SFR (also see Glazebrook et al. 1999). However, we observe the same excess $H\alpha$ emission (relative to UV) in a sample that is dominated by normal star-forming disk galaxies, with no evidence for current or recent starbursts. This implies that temporal variations in SFRs cannot account for the inconsistency in SFRs, at least not in our sample, and instead we tentatively attribute the difference to higher attenuation of the FUV emission relative to $H\alpha$ (as suggested by e.g. Glazebrook et al. 1999; Yan et al. 1999; Moorcroft et al. 2000). In §4 we compare the FUV and $H\alpha$ attenuations directly and confirm this tentative conclusion. Although temporal effects may play a role in accounting for the systematic difference in $H\alpha$ and FUV SFRs observed in high-redshift galaxies, our results strongly suggest that dust extinction effects should not be ruled out.

4. EFFECTS OF DUST ATTENUATION

Dust attenuation strongly affects the optical and UV radiation from star-forming galaxies, as evidenced by the large fractional FIR luminosities of most spiral galaxies (Xu & Buat 1995), by the substantial reddenings of the Balmer lines in the brightest H II regions and in the integrated spectra of the galaxies themselves (e.g. Kennicutt 1992; Zaritsky et al. 1994; Wang & Heckman 1996), and by the observed correlations between UV spectral slope and FUV vs FIR properties of galaxies (Calzetti et al. 1994; Heckman et al. 1998; Meurer et al. 1995; Meurer, Heckman, & Calzetti 1999). In the previous section we tentatively attributed the factor of 1.5 discrepancy between uncorrected UV

and $H\alpha$ -derived SFRs to excess attenuation in the ultraviolet; in this section we derive direct constraints on the FUV and $H\alpha$ attenuations to test this hypothesis. We deliberately apply some of the methods that are most commonly applied to high-redshift objects, so we can use the UIT sample to assess the reliability of these extinction correction schemes when independent information on the SFRs is available.

4.1. Constraints on FUV Attenuation

The most common methods that been employed to estimate UV attenuation in external galaxies are to scale the attenuation by the mean column density of H I (or H I + H₂) gas (Donas & Deharveng 1984; Donas et al. 1987), or to apply an empirical correlation between the UV spectral slope, Balmer decrement, and total attenuation (e.g. Calzetti et al. 1994). More recent work on the use of column densities to predict UV attenuation shows a disappointing scatter (Buat 1992; Buat & Xu 1996), and most workers estimate the extinction corrections using the spectral slope method. We have used the empirical attenuation curve determined for a sample of 39 starburst galaxies by Calzetti et al. (1994) to derive approximate FUV attenuation corrections for our sample.

The Calzetti et al. (1994) method effectively uses an empirically determined extinction law to relate the attenuation at a given wavelength to the slope of the UV spectral energy distribution. In order to measure the spectral slopes of our galaxies we measured the NUV magnitudes of a subsample of 15 galaxies (13 of which have FUV magnitudes also) which were observed using Astro-1. We then used the FUV and NUV magnitudes of these 13 galaxies to determine the slope of their UV continuum β , following Calzetti et al. We have then applied their method to determine the FUV attenuation at 1567 \AA A_{FUV} :

$$A_{\text{FUV}} = 0.5k_{\lambda}(\beta + 1.71)/1.88, \quad (4)$$

where $k_{\lambda} = 8.66$ at 1567 \AA (Calzetti et al. 1994).

Although this analysis allows us to characterize the approximate FUV extinction properties of our (sub)sample, the derived attenuations are very sensitive to small errors in the FUV – NUV colors, and hence the values derived for individual objects are not very meaningful. Another concern is that the relation given above was determined using small-aperture observations of a sample of UV-bright starburst galaxies, and it may not be entirely appropriate for normal star-forming galaxies over a wide range in mass and SFR. In particular, Witt & Gordon (2000) show that FUV color-based extinction estimates are strongly sensitive to the shape of the FUV extinction curve, and that Calzetti et al.'s (1994) attenuation law necessitates a SMC bar-type extinction curve (although see Granato et al. (2000) for a different viewpoint). Therefore, a FUV color-based attenuation may not be appropriate for spiral galaxies: we test this in §4.4.

4.2. $H\alpha$ Attenuation Measurements

To calculate the attenuation at $H\alpha$ ($A_{H\alpha}$), we combined our $H\alpha$ fluxes with thermal radio continuum fluxes for a subset of 16 UIT and 5 FAUST galaxies with reliable radio data. The two fluxes are directly correlated, with only a weak dependence on nebular electron temperature: $\Delta A_{H\alpha} = 1.475 \log_{10}(T_e/10^4 \text{ K})$, where for a reasonable range in true H II region electron temperature T_e from 8000K to 12000K the error in the attenuation estimate is ∓ 0.15 mag (Condon 1992). We assume $T_e = 10000\text{K}$. Following Condon (1992), we translate the thermal radio flux into an $H\alpha$ luminosity via:

$$L_{H\alpha, \text{predicted}} (\text{ergs s}^{-1}) = 8.3 \times 10^{13} L_{\text{thermal}} (\text{ergs s}^{-1} \text{ Hz}^{-1}) \quad (5)$$

where $L_{H\alpha, \text{predicted}}$ is the predicted $H\alpha$ luminosity from a given thermal radio continuum luminosity at 1.4 GHz L_{thermal} .

As is the case with the FUV attenuations derived from the β method, the $H\alpha$ attenuations derived in this way are subject to large uncertainties for individual galaxies, in this case due to the errors associated with separating the non-thermal and thermal components to the radio luminosity (see §2.2).

One common method for estimating the attenuation at $H\alpha$ is to compare the ratio of the $H\alpha$ and $H\beta$ fluxes with the theoretical value of 2.86 (at $T_e = 10000$ K; Caplan & Deharveng 1986). This gives the reddening between $H\alpha$ and $H\beta$: with the assumption of an attenuation curve it is possible to then estimate the attenuation at $H\alpha$, or indeed, any other wavelength. This approach has known limitations. Generally, Balmer decrement measurements are only available for bright H II regions within the galaxies, and applying this mean extinction to the galaxy as a whole is a rough approximation at best. Moreover, the radio-derived attenuation of H II regions in the LMC are larger than those expected from the Balmer decrements using a naive screen model, indicating a grayer extinction curve (probably due to the effects of geometry; e.g. Caplan & Deharveng 1986). This method is commonly used despite its limitations as both $H\alpha$ and $H\beta$ are easily accessible, observationally speaking, and often can even be measured off of the same spectrum (thus minimizing e.g. aperture mismatches or calibration uncertainties).

We have constructed $H\alpha/H\beta$ ratios for 16 UIT and FAUST galaxies with radio-based $H\alpha$ attenuations. These were derived either from spectra of either the entire galaxy (e.g. Kennicutt 1992) or are the average of published $H\alpha/H\beta$ for individual H II regions. These $H\alpha/H\beta$ values are converted into an attenuation estimate assuming an intrinsic $H\alpha/H\beta$ of 2.86, and assuming a galactic dust screen model. We find that the $H\alpha$ attenuations derived from radio data are somewhat larger on average than the $H\alpha$ attenuations derived from Balmer decrements (0.2 ± 0.2 mag), with a scatter of nearly 0.8 mag. This modest offset is consistent with a grayer extinction curve, as found by Caplan & Deharveng (1986) for H II regions in the LMC. Given the modest numbers of galaxies with Balmer decrements, and bearing in mind the systematic uncertainties inherent to Balmer decrement-based attenuations, we do not consider these further, except to note that these attenuations are consistent with the radio-based values, with much scatter.

4.3. Comparison of FUV and $H\alpha$ Attenuation Distributions

We compare the FUV and $H\alpha$ attenuation distributions in Fig. 3 for the respective subsamples of 13 and 21 galaxies. Arrows denote the median attenuation. The two galaxies with derived $A_{FUV} > 6$ mag (NGC 2551, NGC 3034) have spectral slopes $\beta > 0$, and lie outside the calibration range of Calzetti et al. (1994).

Figure 3 shows that the distributions of $H\alpha$ and 1567 Å FUV attenuations are qualitatively similar. The median FUV attenuation is 1.4 mag as compared to 0.9 mag for $H\alpha$. The somewhat higher FUV attenuations are consistent with the systematic offset in uncorrected SFRs discussed earlier, although the formal uncertainties in the median values are roughly ± 0.3 mag in both cases, so the difference between $H\alpha$ and FUV values is only marginally significant. Furthermore, these samples only have two galaxies in common (NGC 3031 and NGC 3034), so it is dangerous to draw any firm conclusions from the relative attenuation distributions.

4.4. Comparison with FIR Properties

One interesting question is whether or not there is evidence against a single, representative attenuation for our sample of star-forming galaxies. In other words, is the spread in the attenuations in Fig. 3 just a random scatter, or does the spread indicate a systematic variation in spiral galaxy attenuation? There is already ample evidence for an increase in UV attenuation with increasing FIR luminosity (e.g. Wang & Heckman 1996; Meurer, Heckman, & Calzetti 1999; Buat et al. 1999). However, there has been no evidence for an increase in $H\alpha$ attenuation as a function of FIR luminosity: there is evidence for increased $H\alpha$ reddening (Calzetti et al. 1994; Wang & Heckman 1996) or a decreased $H\alpha$ to FIR luminosity ratio with FIR luminosity (Cram et al. 1998), but no direct evidence for a change in $H\alpha$ attenuation.

To test for systematically varying attenuation in these galaxies, Fig. 4 plots the color-based FUV and $H\alpha$ attenuations derived above against a different indicator of UV attenuation: the FIR to FUV luminosity ratio. This ratio is subject to its own set of systematic uncertainties (e.g. the possible influence of old stellar population heating of the dust, the assumption of a flat FUV spectrum in terms of flux per unit frequency, or dust heating from ionizing FUV radiation), however the FIR/FUV should suffice to rank galaxies roughly by the amount of UV attenuation, at the very least.

In Fig. 4, we show the 1567 Å FUV (panel a) and $H\alpha$ (panel b) attenuations against FIR/FUV. The solid line denotes the expected relationship if the FIR luminosity was produced solely by absorption of FUV radiation, and if the attenuation at $H\alpha$ was half as large as that at 1567 Å. Dotted lines denote the relationship if the $H\alpha$ attenuation was as large (upper line) or only a quarter as large (lower line) as the FUV attenuation. In panel a, we can see that the evidence for a correlation between the UV spectral slope-based attenuation and FIR/FUV is inconclusive. This may indicate that while β for spiral galaxies may give a rough measure of the FUV attenuation, it may not be accurate on a case-by-case basis (perhaps due to variation in the shape of the FUV attenuation curves). However, only six of the thirteen galaxies have both accurate A_{FUV} and FIR/FUV values: five galaxies lack significant FIR detections (we plot these galaxies with $\log_{10}(\text{FIR}/\text{FUV}) \sim -1$ as they are likely to have reasonably low FIR/FUV), and the other two galaxies have UV spectral slopes outside the calibration range of Calzetti et al. (1994). Clearly more NUV and FUV magnitudes of a larger sample of galaxies are required to properly address this question with any degree of certainty.

In contrast, the $H\alpha$ attenuations (panel b; determined from the $H\alpha$ to thermal radio continuum ratio, for galaxies where the thermal radio was detected at better than 1σ) appear to correlate more strongly with FIR/FUV. Somewhat surprisingly, the solid line, which denotes the relationship between attenuation and FIR/FUV (assuming that the $H\alpha$ attenuation is half of that in the FUV, and assuming that FIR/FUV is essentially a FUV attenuation indicator for this sample) describes the data rather well. This should be taken with some caution, as there is likely a contribution to the dust heating from older stellar populations (or absorption of the ionizing continuum before it can ionize hydrogen in H II regions), which would add scatter and/or a systematic bias to this comparison.

Despite the modest sample size, the correlation between $A_{H\alpha}$ and FIR/FUV dispels the notion of a constant $H\alpha$ attenuation: there is a large range of attenuations in star-forming galaxies,

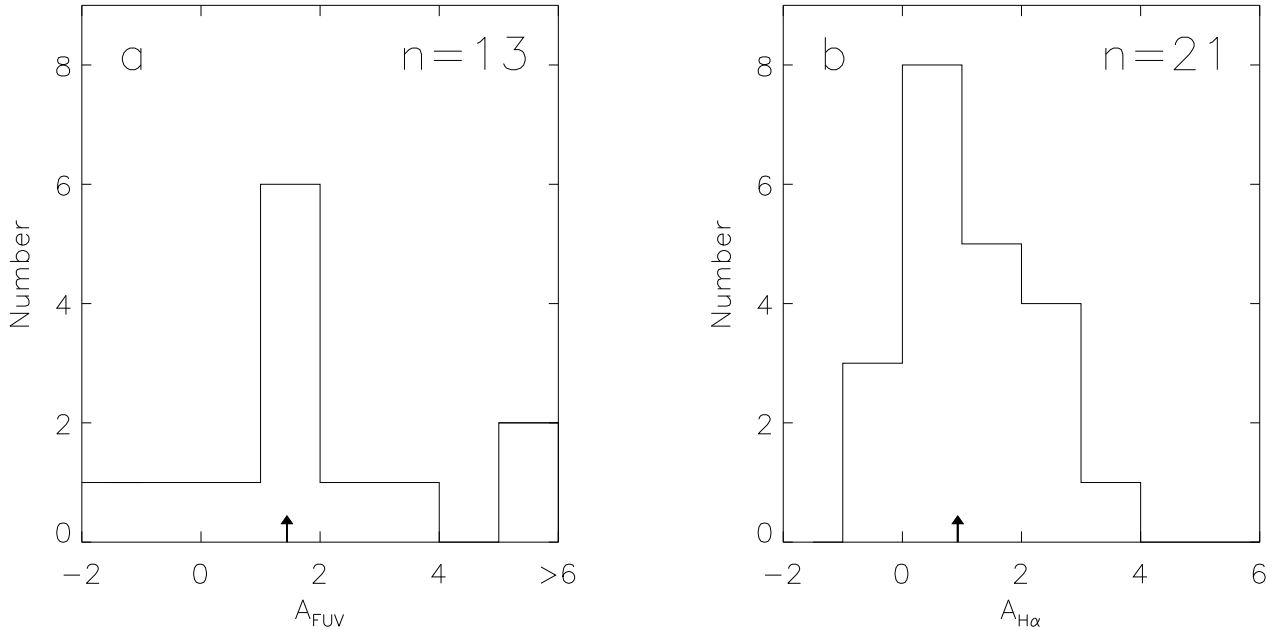


FIG. 3.— Distributions of the FUV (panel a) and H α (panel b) attenuations for two different subsamples of 13 and 21 galaxies respectively. Arrows denote the median attenuation.

and the H α and UV attenuation in a given galaxy are at least loosely correlated. Furthermore, the range in H α attenuations is at least 4 mags in our sample of galaxies, indicating that emission line-based SFR estimates of very highly obscured galaxies may be up to 1 or 2 orders of magnitude lower than the true SFRs. The UV is affected by more attenuation, and the problem may be even more severe for the UV-based SFRs of highly obscured galaxies. This scenario is qualitatively consistent with that outlined in by e.g. Buat et al. (1999), Wang & Heckman (1996), or Heckman et al. (1998) where more massive, higher SFR galaxies have more attenuation. This would explain the factor of 1.5 offset between H α and FUV SFRs for high luminosity galaxies (in this picture, low luminosity galaxies have comparable SFRs in the H α and FUV because the effects of dust are small for both SFR indicators), and the curve in panel b of Fig. 4. Furthermore, this scenario is roughly consistent with the distributions of FUV and H α attenuations in Fig. 3.

5. CONCLUSIONS

We have performed photometry on UIT NUV and FUV images of a sample of 50 star-forming galaxies. Comparison with literature FUV magnitudes suggests that our magnitudes are accurate to better than 0.4 mag. Combining these NUV and FUV magnitudes with literature H α , FIR, and thermal radio continuum measurements, we have found the following.

- Raw FUV and H α SFR estimates are consistent to within a factor of two. At low luminosities, H α SFR estimates are around 25% lower than FUV SFR estimates, indicating either inconsistencies in the SFR calibrations, or the effects of low-level bursts of star formation. At higher luminosities, H α SFR estimates are ~ 1.5 times higher than FUV SFR estimates, with a factor-of-two scatter. This indicates that FUV attenuation is, on average, larger than H α attenuation.

Furthermore, the difference in H α to FUV SFR ratio between high and low luminosity galaxies suggests that there are differences in extinction properties which correlate at least loosely with luminosity.

- For subsets of our sample of galaxies, we have constructed FUV attenuation estimates using the UV spectral slope as an attenuation indicator (Calzetti et al. 1994), and H α attenuation estimates by comparing H α and thermal radio continuum luminosities. The median FUV attenuation is somewhat larger than the median H α attenuation, although with marginal significance.
- Comparison of the H α attenuation with the FIR/FUV for our galaxies demonstrates that there is a broad range in H α attenuation. If FIR/FUV is driven mainly by attenuation, there are suggestions that the H α attenuation correlates broadly with the FUV attenuation, and is around a factor of two lower than the FUV attenuation.
- A characteristic H α and FUV attenuation for our sample of galaxies is ~ 0.9 mag and ~ 1.4 mag respectively, although there is a large range in attenuations in our sample, ranging from 0 to 4 magnitudes at H α .

We thank Karl Gordon for providing the total IR estimation IDL routine, and for numerous helpful discussions. We acknowledge useful suggestions from and discussions with Mark Sullivan, Richard Ellis, Gerhardt Meurer, and especially the anonymous referee. This work was supported by NASA grant NAG5-8426 and NSF grant AST-9900789. Some of the data presented in this paper was obtained from the Multimission Archive at the Space Telescope Science Institute (MAST). STScI

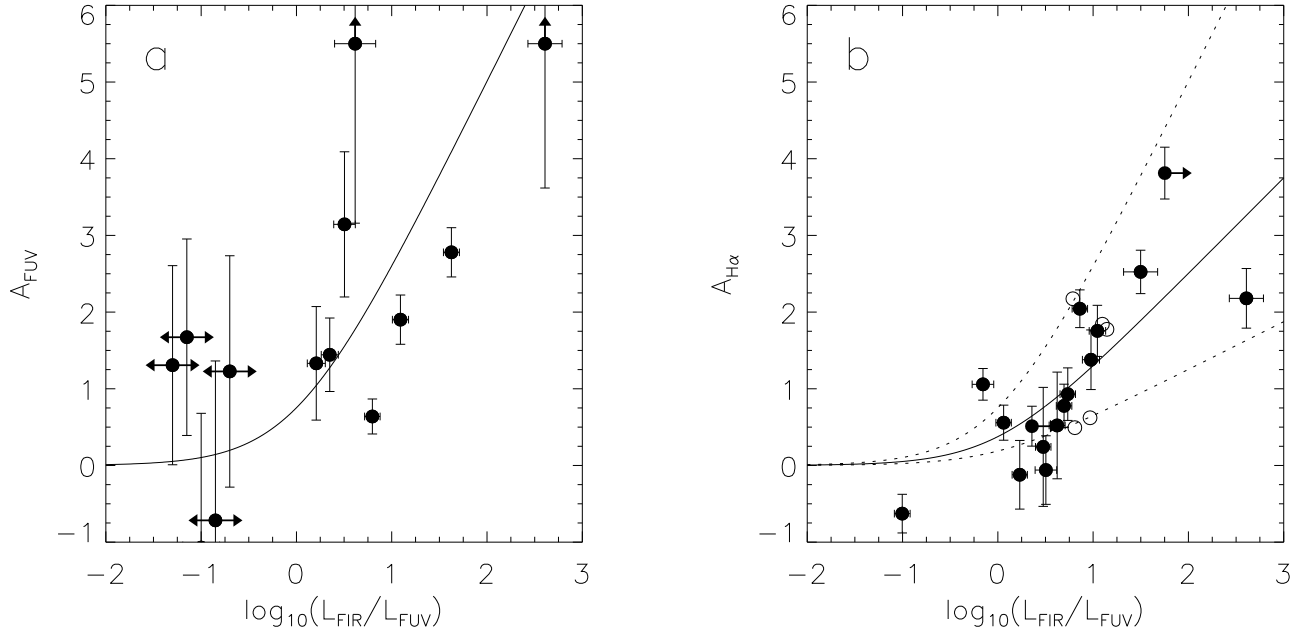


FIG. 4.— Comparison of the FUV (panel a) and $H\alpha$ (panel b) attenuation with FIR/FUV. Arrows in panel a denote galaxies without FIR luminosities; however, these galaxies are likely on the whole to have low FIR/FUV (and have A_{FUV} values which are consistent with zero in any case). Arrows in panel b denote FUV luminosity upper limits. The solid line shows the expected relationship if the FIR luminosity was produced solely by absorption of FUV radiation, and produced an attenuation at $H\alpha$ half as large as that at 1567 \AA . Dotted lines denote the relationship if the $H\alpha$ attenuation was as large (upper line) or only a quarter as large (lower line) as the FUV attenuation.

is operated by the Association of Universities for Research in Astronomy, Inc., under NASA contract NAS5-26555. Support for MAST for non-HST data is provided by the NASA Office of Space Science via grant NAG5-7584 and by other grants and contracts. This research has made extensive use of the NASA/IPAC Extragalactic Database (NED) which is operated by the Jet Propulsion Laboratory, California Institute of Technology, under contract with the National Aeronautics and Space Administration.

REFERENCES

- Broadhurst, T. J., Ellis, R. S., Shanks, T. S., 1988, *MNRAS*, 235, 827
 Buat, V., Donas, J., Deharveng, J.M. 1987, *A&A*, 185, 33
 Buat, V., 1992, *A&A*, 264, 444
 Buat, V., Xu, C., 1996, *A&A*, 306, 61
 Buat, V., Donas, J., Milliard, B., Xu, C., 1999, *A&A*, 352, 371
 Bushouse, H. A., Werner, M. W., Lamb, S. A., 1988, *ApJ*, 335, 74
 Caldwell, N., Kennicutt Jr., R. C., Phillips, A. C., Schommer, R. A., 1991, *ApJ*, 370, 526
 Calzetti, D., Kinney, A. L., Storchi-Bergmann, T., 1994, *ApJ*, 429, 582
 Caplan, J., Deharveng, L., 1986, *A&A*, 155, 297
 Carlstrom, J. E., Kronberg, P. P., 1991, *ApJ*, 366, 422
 Ciardullo, R., Jacoby, G. H., Harris, W. E., 1991, *ApJ*, 383, 487
 Code, A. D., Welch, G. A., 1982, *ApJ*, 256, 1
 Condon, J. J., Helou, G., Sanders, D. B., Soifer, B. T., 1990, *ApJS*, 73, 359
 Condon, J. J., 1992, *ARA&A*, 30, 575
 Cram, L., Hopkins, A., Mobasher, B., Rowan-Robinson, M., 1998, *ApJ*, 507, 155
 Crocker, D. A., Baugus, P. D., Buta, R., 1996, *ApJS*, 105, 353
 Deharveng, J. M., Sasseen, T. P., Buat, V., Bowyer, S., Lampton, M., Wu, X., 1994, *A&A*, 289, 715
 de Vaucouleurs, A., Longo, G., 1988, *Catalogue of Visual and Infrared Photometry of Galaxies from 0.5 micron to 10 micron (1961-1985)* (Austin, University of Texas)
 de Vaucouleurs, G., de Vaucouleurs, A., Corwin Jr., H. G. Buta, R. J., Paturel, G., Fouque, P., 1991, *Third Reference Catalogue of Bright Galaxies, version 3.9* (New York, Springer Verlag) (RC3)
 Dohm-Palmer, R., et al. 1998, *AJ*, 114, 2527
 Donas, J., Deharveng, J. M., 1984, *A&A*, 140, 325
 Donas, J., Deharveng, J. M., Laget, M., Milliard, B., Huguenin, D., 1987, *A&A*, 180, 12
 Donas, J., Buat, V., Milliard, B., Laget, M., 1990, *A&A*, 235, 60
 Duric, N., Bourneuf, E., Gregory, P. C., 1988, *AJ*, 96, 81
 Gallego, J., Zamorano, J., Aragon-Salamanca, A., Rego, M., 1995, *ApJ*, 455, 1L
 Garnier, R., Paturel, C., Petit, C., Marthinet, M. C., Rousseau, J., 1996, *A&AS*, 117, 467
 Gavazzi, G., Catinella, B., Carrasco, L., Boselli, A., Contursi, A., 1998, *AJ*, 115, 1745
 Glazebrook, K., Blake, C., Economou, F., Lilly, S., Colless, M., 1999, *MNRAS*, 306, 843
 González Delgado, R. M., Leitherer, C., Heckman, T., Lowenthal, J. D., Ferguson, H. C., Robert, C., 1998, *ApJ*, 495, 698
 Gordon, K. D., Calzetti, D., Witt, A. N., 1997, *ApJ*, 487, 625
 Gordon, K. D., Clayton, G. C., Witt, A. N., Misselt, K. A., 2000, *ApJ*, 533, 236
 Granato, G. L., Lacey, C. G., Silva, L., Bressan, A., Baugh, C. M., Cole, S., Frenk, C. S., 2000, *ApJ*, in press (astro-ph/0001308)
 Heckman, T. M., Robert, C., Leitherer, C., Garnett, D. R., van der Rydt, F., 1998, *ApJ*, 503, 646
 Helou, G., Soifer, B. T., Rowan-Robinson, M., 1985, *ApJ*, 298, L7
 Hoopes, C. G., Walterbos, R. A. M., Greenwalt, B. E., 1996, *AJ*, 112, 1429
 Hoopes, C. G., Walterbos, R. A. M., Rand, R. J., 1999, *ApJ*, 522, 669
 Huchra, J. P., 1977, *ApJS*, 35, 171
 Hummel, E., van der Hulst, J. M., Keel, W. C., 1987, *A&A*, 172, 32
 Hunter, D. A., Plummer, J. D., 1996, *ApJ*, 462, 732
 Hutchings, J. B., Neff, S. G., Stanford, S. A., Lo, E., Unger, S. W., 1990, *AJ*, 100, 60
 Iglesias-Páramo, J., Vílchez, J. M., 1999, *ApJ*, 518, 94
 Karachentsev, I. D., Sharina, M. E., 1997, *A&A*, 324, 457
 Kennicutt Jr., R. C., 1983, *ApJ*, 272, 54
 Kennicutt Jr., R. C., 1992, *ApJ*, 388, 310
 Kennicutt Jr., R. C., 1998, *ARA&A*, 36, 189
 Kennicutt Jr., R. C., Kent, S. M., 1983, *AJ*, 88, 1094
 Kennicutt Jr., R. C., Bothun, G. D., Schommer, R. A., 1984, *AJ*, 89, 1279
 Kennicutt Jr., R. C., Keel, W. C., van der Hulst, J. M., Hummel, E., Roettiger, K. A., 1987, *AJ*, 93, 1011
 Kirshner, R. P., Oemler Jr., A., Schechter, P. L., 1978, *AJ*, 83, 1549
 Klein, U., Hummel, E., Bomans, D. J., Hopp, U., 1996, *A&A*, 313, 396
 Kuchinski, L. E., Freedman, W. L., Madore, B. F., Trewhella, M., Bohlin, R. C., Cornett, R. C., 2000, *ApJS*, in press (astro-ph/0002111)
 Kühr, H., Witzel, A., Pauliny-Toth, I. I. K., Nauber, U., 1981, *A&AS*, 45, 367

- Lauberts, A., Valentijn, E. A., 1989, The Surface Photometry Catalogue of the ESO-Uppsala Galaxies (Garching bei München, ESO)
- Leitherer, C., et al., 1999, ApJS, 123, 3
- Lilly, S. J., 1993, ApJ, 411, 502
- Madau, P., Pozzetti, L., Dickinson, M., 1998, ApJ, 498, 106
- Marcum, P. M., et al., 2000, ApJS, in press
- Martin, C. L., 1998, ApJ, 506, 222
- McQuade, K., Calzetti, D., Kinney, A. L., 1995, ApJS, 97, 331
- Melisse, J. P. M., Israel, F. P., 1994, A&AS, 103, 391
- Meurer, G. R., Heckman, T. M., Leitherer, C., Kinney, A., Robert, C., Garnett, D. R., 1995, AJ, 110, 2665
- Meurer, G. R., Heckman, T. M., Calzetti, D., 1999, ApJ, 521, 64
- Miller, B. W., Hodge, P., 1994, ApJ, 427, 656
- Moorcroft, A. F. M., van der Werf, P. P., Cuby, J. G., Oliva, E., 2000, A&A, in press (astro-ph/0009010)
- Moshir, M., et al., 1990, IRAS Faint Source Catalogue, version 2.0 (Pasadena, IPAC)
- Moss, C., Whittle, M., Pesce, J. E., 1998, MNRAS, 300, 205
- Niklas, S., Klein, U., Wielebinski, R., 1997, A&A, 322, 19
- Puche, D., Carignan, C., 1988, AJ, 95, 1025
- Rice, W., Lonsdale, C. J., Soifer, B. T., Neugebauer, G., Kopan, E. L., Lloyd, L. A., de Jong, T., Habing, H. J., 1988, ApJS, 68, 91
- Rifatto, A., Longo, G., Capaccioli, M., 1995, A&AS, 114, 527
- Ryder, S. D., Dopita, M. A., 1994, ApJ, 430, 142
- Sakai, S., Madore, B. F., Freedman, W. L., 1996, ApJ, 461, 713
- Salpeter, E. E., 1955, ApJ, 121, 61
- Sandage, A., Tammann, G. A., 1974, ApJ, 191, 603
- Schlegel, D. J., Finkbeiner, D. P., Davis, M., 1998, ApJ, 500, 525
- Shanks, T., 1997, MNRAS, 290, 77L
- Soifer, B. T., Boehmer, L., Neugebauer, G., Sanders, D. B., 1989, AJ, 98, 766
- Stecher, T. P., Cornett, R. H., Greason, M. R., Landsman, W. B., Hill, J. K., Hill, R. S., et al., 1997, PASP, 109, 584
- Steidel, C. C., Adelberger, K. L., Giavalisco, M., Dickinson, M., Pettini, M., 1999, ApJ, 519, 1
- Sullivan, M., Treyer, M. A., Ellis, R. S., Bridges, T. J., Milliard, B., Donas, J., 2000, MNRAS, 312, 442
- Tongue, T. D., Westpfahl, D. J., 1995, AJ, 109, 2462
- Tolstoy, E., et al., 1998, AJ, 116, 1244
- Tresse, L., Maddox, S. J., 1998, ApJ, 495, 691
- Usui, T., Saitō, M., Tomita, A., 1998, AJ, 116, 2166
- Waller, W. H., Marsh, M., Bohlin, R. C., Cornett, R. H., Dixon, W. V., Isensee, J. E., et al., 1995, AJ, 110, 1255
- Waller, W. H., et al., 1997, in AIP Conf. Proc. 408, The Ultraviolet Universe at Low and High Redshift: Probing the Progress of Galaxy Evolution, ed. W. H. Waller, M. N. Fanelli, J. E. Hollis, & A. C. Danks (Woodbury, New York: AIP), 39
- Wang, B., Heckman, T. M., 1996, ApJ, 457, 645
- Witt, A. N., Gordon, K. D., 2000, ApJ, 528, 799
- White, R. L., Becker, R. M., 1992, ApJS, 79, 331
- Wright, A., Otrupcek, R., 1990, Parkes Catalogue, (Parkes, ATNF)
- Xu, C., Buat, V., 1995, A&A, 293, L65
- Yan, L., McCarthy, P. J., Freudling, W., Teplitz, H. I., Malumuth, E. M., Weymann, R. J., Malkan, M. A., 1999, ApJ, 519, L47
- Young, J. S., Xie, S., Kenney, J. D. P., Rice, W. L., 1989, ApJS, 70, 699
- Young, J. S., Allen, L., Kenney, J. D. P., Lesser, A., Rownd, B., 1996, AJ, 112, 1903
- Zaritsky, D., Kennicutt, R. C., Huchra, J. P. 1994, ApJ, 420, 87

TABLE I
SAMPLE PROPERTIES

Galaxy Name	Alternative Name	RA (2000) hh mm ss	Dec (2000) dd mm ss	RC3 Type	D (Mpc)	Dist Ref	Galactic A_V
NGC 253	...	00 47 33.1	-25 17 18	SAB(s)c; H II	2.6	8	0.06
NGC 628	M74	01 36 41.7	15 46 59	SA(s)c	10.0	1	0.23
NGC 891	...	02 22 33.4	42 20 57	SA(s)b; pec	9.9	5	0.22
NGC 925	...	02 27 17.0	33 34 43	SAB(s)d	8.9	1	0.25
NGC 1068	M77	02 42 40.7	-00 00 48	(R)SA(rs)b; Sy	15.1	1	0.11
NGC 1097	...	02 46 19.1	-30 16 28	(R)SB(r)b; Sy	15.9	1	0.09
NGC 1291	NGC 1269	03 17 18.3	-41 06 28	(R)SB(l)0/a	8.6	7	0.04
NGC 1313	...	03 18 15.4	-66 29 51	SB(s)d; H II	3.9	1	0.37
NGC 1317	...	03 22 44.4	-37 06 13	(R)SAB(rl)0/a	20	11	0.07
NGC 1365	...	03 33 36.4	-36 08 25	(R)SBb(s)b; Sy	20.5	1	0.07
NGC 1512	...	04 03 54.3	-43 20 57	SB(r)ab	9.8	1	0.04
NGC 1566	...	04 20 00.6	-54 56 17	(R)SAB(rs)bc; Sy	17.6	1	0.03
NGC 1672	...	04 45 42.1	-59 14 57	(R)SB(r)bc; Sy	15.4	1	0.08
NGC 2146	...	06 18 39.7	78 21 23	SB(s)ab; pec	14.5	6	0.32
NGC 2403	...	07 36 51.4	65 36 09	SAB(s)cd; H II	3.0	1	0.13
NGC 2551	...	08 24 50.2	73 24 44	SA(s)0/a	31	3	0.09
NGC 2841	...	09 22 02.7	50 58 36	SA(r)b; LINER/Sy	9.0	1	0.05
NGC 2903	...	09 32 10.1	21 30 04	SB(s)d; H II	6.3	1	0.10
NGC 2993	...	09 45 43.8	-14 22 05	Sa pec	32	3	0.20
NGC 3031	M81	09 55 33.2	69 03 55	SA(s)ab; LINER/Sy	3.3	1	0.27
NGC 3034	M82	09 55 52.2	69 40 47	l0; H II	3.3	1	0.53
NGC 3310	...	10 38 45.9	53 30 12	SAB(r)bc pec; H II	13.9	1	0.07
NGC 3351	M95	10 43 58.0	11 42 14	SB(r)B; H II	9.0	1	0.09
NGC 3389	...	10 48 27.9	12 32 00	SA(s)c	24	10	0.09
NGC 4038/9	The Antennae	12 01 55.2	-18 52 44	Pec/int	19.8	1	0.15
NGC 4156	...	12 10 49.6	39 28 22	SB(rs)b; LINER	90	3	0.09
NGC 4214	...	12 15 38.7	36 19 42	IAB(s)m; H II	4.2	1	0.07
NGC 4258	M106	12 18 57.5	47 18 14	SAB(s)bc; LINER/Sy	6.8	1	0.05
NGC 4321	M100	12 22 54.9	15 49 21	SAB(s)bc; LINER/H II	16.0	1	0.09
NGC 4449	...	12 28 12.0	44 05 41	IBm; H II	3.4	1	0.06
NGC 4631	...	12 42 05.9	32 32 22	SB(s)d	8.4	1	0.06
NGC 4647	...	12 43 32.3	11 34 55	SAB(rs)c	20	11	0.09
NGC 4736	M94	12 50 53.1	41 07 14	(R)SA(r)ab; LINER	4.8	1	0.06
NGC 5055	M63	13 15 49.3	42 01 49	SA(rs)bc; H II/LINER	7.6	1	0.06
NGC 5194	M51	13 29 52.3	47 11 54	SA(s)bc pec; H II/Sy	7.3	1	0.12
NGC 5236	M83	13 37 00.8	-29 51 59	SAB(s)c; H II	3.7	1	0.22
NGC 5253	...	13 39 55.9	-31 38 24	Im pec; H II	3.6	1	0.19
NGC 5457	M101	14 03 12.5	54 20 55	SAB(rs)cd	7.4	1	0.03
NGC 6090	Mrk 496	16 11 40.3	52 27 26	Pec/int	117	3	0.07
NGC 6946	...	20 34 52.3	60 09 14	SAB(rs)cd; H II	6.2	9	1.13
DDO 50	Holmberg II	08 19 06.0	70 42 51	Im	3.1	2	0.11
DDO 66	Holmberg IX	09 57 32.4	69 02 35	Im	3.3	1	0.26
DDO 75	Sextans A	10 11 00.8	-04 41 34	IBm	1.45	4	0.15
DDO 81	IC 2574	10 28 21.2	68 24 43	SAB(s)m	3.1	2	0.12
UGC 6697	...	11 43 49.2	19 58 05	Im	90	3	0.07
UGC 7188	...	12 11 16.4	39 24 08	SBm	13	3	0.08
CGCG 097-093	...	11 44 01.9	19 47 04	Irr	66	3	0.07
CGCG 097-114	...	11 44 47.7	19 46 27	Irr	111	3	0.08
Mrk 66	...	13 25 53.7	57 15 05	BCG	87	3	0.04
IRAS 08339+6517	...	08 38 23.4	65 07 14	Pec; H II	76	3	0.31

References. — (1) Waller et al. (1997) (2) Sandage & Tammann (1974) (3) Hubble flow assuming $H_0 = 75 \text{ km s}^{-1} \text{ Mpc}^{-1}$ (4) Sakai, Madore, & Freedman (1996) (5) Ciardullo, Jacoby, & Harris (1991) (6) Hutchings et al. (1990) (7) Crocker, Baugus, & Buta (1996) (8) Puche & Carignan (1988) (9) Karachentsev & Sharina (1997) (10) Shanks (1997) (11) Distance to the Virgo and Fornax Clusters, following Shanks (1997)

TABLE 2
UV EXPOSURE TIMES

Galaxy Name	Far-UV		Near-UV
	B1 (s)	B5 (s)	A1 (s)
NGC 253	...	275.5	...
NGC 628	514.5	...	530.5
NGC 891	437.5,380.5	...	437.5
NGC 925	...	1590.5	...
NGC 1068	752.5,563.5	987.5,752.5	563,129
NGC 1097	...	1120.5,605.5	...
NGC 1291	...	1590.5	...
NGC 1313	...	1070.5	...
NGC 1317	545.5	545.5	545.5
NGC 1365	...	973.5	...
NGC 1512	...	948.5	...
NGC 1566	...	1390.5	...
NGC 1672	...	926.5	...
NGC 2146	442.5	443.5	442.5
NGC 2403	771.5
NGC 2551	1060.5	451.5	454.5
NGC 2841	1020.5
NGC 2903	548.5,348.5
NGC 2993	256.5	541.5	256.5
NGC 3031	640.5	...	639.5
NGC 3034	270.5	...	270.5
NGC 3310	1130.5
NGC 3351	880.7
NGC 3389	1300.5
NGC 4038/9	880.5
NGC 4156	832.5,804.5	1199.5	239.5
NGC 4214	1060.5
NGC 4258	1310.5
NGC 4321	...	226.5	...
NGC 4449	986.7	493.5	...
NGC 4631	1140.5	1560.5	...
NGC 4647	1300.5
NGC 4736	1040.5
NGC 5055	1140.5
NGC 5194	1100.5
NGC 5236	818.5	1430.5	...
NGC 5253	725.7	726.5	...
NGC 5457	1310.5
NGC 6090	966.5,842.5
NGC 6946	...	546.5	...
DDO 50	1310.5
DDO 66	640.5	...	639.5
DDO 75	689.5
DDO 81	623.5
UGC 6697	753.5	529.5	105.5
UGC 7188	832.5,804.5	1199.5	239.5
CGCG 097-093	753.5	529.5	105.5
CGCG 097-114	753.5	529.5	105.5
Mrk 66	775.5
IRAS 08339+6517	1186.5

TABLE 3
ULTRAVIOLET MAGNITUDES

Galaxy Name	B1 Magnitude	B5 Magnitude	A1 Magnitude	Aperture (arcsec)
NGC 253	...	8.3 ± 0.4	...	700
NGC 628	9.7 ± 0.1	...	10.18 ± 0.03	300
NGC 891	$> 12.5 (3\sigma)$...	13.4 ± 0.4	100
NGC 925	...	9.6 ± 0.2	...	400
NGC 1068	10.21 ± 0.05	9.8 ± 0.1	10.35 ± 0.03	200
NGC 1097	...	10.2 ± 0.2	...	250
NGC 1291	...	13.9 ± 0.3	...	70
NGC 1313	...	8.9 ± 0.10	...	300
NGC 1317	13.25 ± 0.05	13.10 ± 0.15	13.66 ± 0.02	40
NGC 1365	...	9.65 ± 0.20	...	300
NGC 1512	...	11.60 ± 0.10	...	100
NGC 1566	...	8.84 ± 0.05	...	300
NGC 1672	...	10.35 ± 0.10	...	200
NGC 2146	$> 12 (3\sigma)$	$> 11 (3\sigma)$	12.9 ± 0.2	200
NGC 2403	8.43 ± 0.06	600
NGC 2551	14.8 ± 0.5	$> 13.5 (3\sigma)$	14.05 ± 0.10	70
NGC 2841	11.0 ± 0.2	250
NGC 2903	10.15 ± 0.08	150
NGC 2993	11.90 ± 0.03	11.95 ± 0.08	12.57 ± 0.03	50
NGC 3031	9.1 ± 0.2	...	9.20 ± 0.05	700
NGC 3034 ^a	12.2 ± 0.4	...	10.97 ± 0.09	150
NGC 3310	9.60 ± 0.03	150
NGC 3351	11.75 ± 0.15	130
NGC 3389	11.70 ± 0.02	100
NGC 4038/9	10.32 ± 0.03	100
NGC 4156	14.3 ± 0.2	14.5 ± 0.3	14.83 ± 0.15	34
NGC 4214	8.92 ± 0.04	300
NGC 4258	9.6 ± 0.2	500
NGC 4321	...	10.2 ± 0.3	...	240
NGC 4449	8.37 ± 0.02	8.45 ± 0.04	...	200
NGC 4631	8.66 ± 0.05	8.55 ± 0.10	...	450
NGC 4647	12.3 ± 0.1	100
NGC 4736	9.31 ± 0.03	200
NGC 5055	9.8 ± 0.1	250
NGC 5194	8.52 ± 0.04	300
NGC 5236	8.01 ± 0.06	7.98 ± 0.03	...	350
NGC 5253	9.80 ± 0.10	9.77 ± 0.10	...	200
NGC 5457	7.39 ± 0.02	800
NGC 6090	13.50 ± 0.03	25
NGC 6946	...	$> 10.2 (3\sigma)$...	250
DDO 50	9.71 ± 0.05	250
DDO 66	14.1 ± 0.2	...	14.6 ± 0.2	75
DDO 75	10.25 ± 0.10	175
DDO 81	9.15 ± 0.15	350
UGC 6697	12.44 ± 0.10	12.6 ± 0.2	13.02 ± 0.10	70
UGC 7188	14.3 ± 0.2	14.4 ± 0.3	15.4 ± 0.3	40
CGCG 097-093	14.62 ± 0.10	14.7 ± 0.3	15.2 ± 0.3	35
CGCG 097-114	14.9 ± 0.4	14.6 ± 0.3	15.7 ± 0.3	30
Mrk 66	13.18 ± 0.06	40
IRAS 08339+6517	12.25 ± 0.05	100

^aNGC 3034 is very faint in the B1 image: only a faint ‘plume’ of far-UV light scattered off of dust is detected (Marcum et al. 2000).

TABLE 4
LUMINOSITIES: STAR FORMATION INDICATORS

Galaxy Name	M_V	UV (10^{27} ergs s^{-1} Hz $^{-1}$)	H α (10^{41} ergs s^{-1})	FIR (10^{43} ergs s^{-1})	Radio (10^{27} ergs s^{-1} Hz $^{-1}$)	Refs
NGC 253	-19.95 ± 0.2^b	1.3 ± 0.5	0.49	8.1	6.1 ± 1.2	5,7,27,33,34,35
NGC 628	-20.84 ± 0.10	8.2 ± 0.8	1.5	3.5	...	1,8,19,27
NGC 891	-20.26 ± 0.18	$< 0.59 (3\sigma)$	0.35	10.6	...	1,9,27
NGC 925	-19.88 ± 0.12	7.5 ± 1.5	0.75	1.00	2.4 ± 0.1	1,19,10,27,36
NGC 1068	-22.14 ± 0.10	9.5 ± 0.6	10.2	77	...	1,8,28
NGC 1097	-21.62 ± 0.07	9.3 ± 1.9	0.83	16.9	...	1,22,27
NGC 1291	-21.25 ± 0.04	0.08 ± 0.02	0.046	0.38	...	1,11,27
NGC 1313	-19.61 ± 0.2	3.6 ± 0.4	0.47	0.70	...	1,23,27
NGC 1317	-20.55 ± 0.06	0.86 ± 0.06	0.26	2.04	...	1,12,28
NGC 1365	-22.00 ± 0.07	24 ± 5	...	46	...	1,27
NGC 1512	-19.67 ± 0.10	0.85 ± 0.09	...	0.53	...	1,28
NGC 1566	-21.53 ± 0.03	35 ± 2	...	7.2	...	1,28
NGC 1672	-21.33 ± 0.08	7.4 ± 0.7	...	9.6	...	1,28
NGC 2146	-20.54 ± 0.13	$< 2.6 (3\sigma)$	1.14	27.9	46 ± 13	1,19,28,37,35
NGC 2403	-19.06 ± 0.08	1.89 ± 0.11	0.49	0.72	...	1,10,27
NGC 2551	-20.43 ± 0.20	0.5 ± 0.25	...	0.41	...	1,28
NGC 2841	-20.60 ± 0.10	1.30 ± 0.25	0.20	1.13	...	1,19,10,27
NGC 2903	-20.09 ± 0.10	1.6 ± 0.1	0.74	3.4	4.5 ± 1.2	1,19,10,27,37,35
NGC 2993	-20.09 ± 0.14	10.2 ± 0.4	2.7	12.3	...	1,24,28
NGC 3031	-20.92 ± 0.03	1.7 ± 0.3	0.45	1.04	0.5 ± 0.2	1,10,27,37,35
NGC 3034	-19.72 ± 0.09	0.19 ± 0.07	1.3	14.6	10 ± 3	1,19,27,38
NGC 3310	-19.99 ± 0.10	11.9 ± 0.4	3.0	6.9	4.6 ± 3.5	1,8,19,29,37,35
NGC 3351	-20.13 ± 0.10	0.72 ± 0.11	0.47	1.60	...	1,8,19,28
NGC 3389	-20.09 ± 0.06	5.3 ± 0.1	1.08	3.0	...	1,8,30
NGC 4038/9	-21.4 ± 0.2	15.1 ± 0.5	6.4	21.1	51 ± 7	2,19,13,29,39,35
NGC 4156	-21.70 ± 0.05	6.5 ± 1.5	1
NGC 4214	-18.41 ± 0.15	2.03 ± 0.08	0.30	0.33	...	1,19,14,29
NGC 4258	-20.81 ± 0.08	2.7 ± 0.5	1.3	1.96	...	1,10,27
NGC 4321	-21.76 ± 0.08	9.4 ± 2.8	2.2	10.3	...	1,19,8,29
NGC 4449	-18.14 ± 0.13	2.14 ± 0.05	0.35	0.47	0.71 ± 0.08	1,8,14,31,40,35
NGC 4631	-20.49 ± 0.16	10.2 ± 0.6	1.83	8.2	3.6 ± 2.4	1,8,9,27,37,35
NGC 4647	-20.30 ± 0.08	2.1 ± 0.2	0.74	4.1	...	1,19,13,29
NGC 4736	-20.22 ± 0.13	1.79 ± 0.05	0.58	1.87	1.6 ± 0.4	1,19,8,27,37,35
NGC 5055	-20.87 ± 0.10	2.9 ± 0.3	0.88	5.2	3.8 ± 1.3	1,8,27,37,35
NGC 5194	-21.07 ± 0.06	9.8 ± 0.4	2.2	9.4	5.5 ± 1.1	1,19,8,40,27,37,35
NGC 5236	-20.52 ± 0.04	5.3 ± 0.2	2.0	5.6	...	1,10,27
NGC 5253	-17.53 ± 0.12	0.88 ± 0.09	0.30	0.53	...	1,21,14,28
NGC 5457	-21.51 ± 0.10	23.1 ± 0.5	3.1	7.6	3.4 ± 1.3	1,10,27,37,35
NGC 6090	-21.34 ± 0.1	22.8 ± 0.7	11.7	96	...	3,20,29
NGC 6946	-21.31 ± 0.11	$< 18 (3\sigma)$	2.6	8.0	5.1 ± 0.9	1,19,10,27,37,35
DDO 50	-16.90 ± 0.17	0.58 ± 0.03	0.044	0.011	0.032 ± 0.005	1,21,15,28,41
DDO 66	-13.76 ± 0.31	0.017 ± 0.003	0.0016	< 0.0050	...	1,21,15,32
DDO 75	-14.48 ± 0.11	0.085 ± 0.008	0.012	0.00061	...	1,16,28
DDO 81	-17.22 ± 0.21	1.00 ± 0.15	0.076	0.043	...	1,15,27
UGC 6697	-21.25 ± 0.10	35 ± 5	5.3	11.0	...	1,17,18,28
UGC 7188	$\sim -16.4 \pm 0.7^c$	0.14 ± 0.03	21
CGCG 097-093	-19.17 ± 0.2	2.6 ± 0.3	0.27	1,25,18
CGCG 097-114	-20.13 ± 0.10	7 ± 2	2.2 ± 0.5	2,25
Mrk 66	-19.75 ± 0.1	16 ± 1	1.1	2.1	...	3,26,28
IRAS 08339+6517	$\sim -21.2 \pm 0.3^a$	54 ± 3	11.2	36	...	4,20,29

References. — (1) de Vaucouleurs et al. (1991) (2) de Vaucouleurs & Longo (1988) (3) Huchra (1977) (4) Kirshner, Oemler, & Schechter (1978) (5) Lauberts & Valentijn (1989) (6) Garnier et al. (1996) (7) Hoopes, Walterbos & Greenwalt (1996) (8) Kennicutt & Kent (1983) times 1.17 (9) Hoopes, Walterbos & Rand (1999) (10) Kennicutt (unpublished) (11) Caldwell et al. (1991) (12) Crocker, Baugus, & Buta (1996) (13) Kennicutt et al. (1987) (14) Martín (1998) (15) Miller & Hodge (1994) (16) Hunter & Plummer (1996) (17) Kennicutt, Bothun, & Schommer (1984) (18) Gavazzi et al. (1998) (19) Young et al. (1996) (20) González Delgado et al. (1998) (21) Iglesias-Páramo & Vílchez (1999) (22) Hummel, van der Hulst, & Keel (1987) (23) Ryder & Dopita (1994) (24) Usui, Saitō, & Tomita (1998) (25) Moss, Whittle, & Pesce (1998) (26) McQuade, Calzetti, & Kinney (1995) (27) Rice et al. (1988) (28) Moshir et al. (1990) (29) Soifer et al. (1989) (30) Bushouse, Werner, & Lamb (1988) (31) Young et al. (1989) (32) Melisse & Israel (1994) (33) Wright & Otrupcek (1990) (34) Kühr et al. (1981) (35) Niklas et al. (1997) (36) Duric, Bourneuf, & Gregory (1988) (37) White & Becker (1992) (38) Carlstrom & Kronberg (1991) (39) Condon et al. (1990) (40) Klein et al. (1996) (41) Tongue & Westpfahl (1995)

^aInterpolated between photographic J and F data: Kirshner, Oemler, & Schechter (1978)

^bAssuming $B-V \sim 1$ from $B-R = 1.52$: Lauberts & Valentijn (1989)

^cAssuming $B-V \sim 0.5$: Garnier et al. (1996)